Topology of spin meron pairs in coupled Ni/Fe/Co/Cu(001) disks

A. Tan, J. Li, A. Scholl, E. Arenholz, A. T. Young, Q. Li, C. Hwang, and Z. Q. Qiu

Phys. Rev. B **94**, 014433 — Published 25 July 2016

DOI: 10.1103/PhysRevB.94.014433

Topology of spin meron pairs in coupled Ni/Fe/Co/Cu(001) disks

A. Tan,[1] J. Li,[2] A. Scholl,[3] E. Arenholz,[3] A. T. Young,[3] Q. Li,[1] C. Hwang,[4] and Z. Q. Qiu[1]

[1] *Dept. of Physics, Univ. of California at Berkeley, Berkeley, CA 94720, USA*
[2] *International Center for Quantum Materials and School of Physics, Peking University, Beijing 100871, China*
[3] *Advanced Light Source, Lawrence Berkeley National Laboratory, Berkeley, CA 94720, USA*
[4] *Korea Research Institute of Standards and Science, Yuseong, Daejeon 305-340, Republic of Korea*

Meron is a special topological object that carries only one-half of the topological charge unit. In condensed matter physics, a spin meron corresponds to one-half of a spin skyrmion. As compared to the many fascinating topological properties of skyrmion materials, little is known of the properties of spin merons especially on their formations. It was confirmed only recently that hedgehog merons could exist in pairs via a spin flux closure with opposite helicities. However, it is unclear on whether a single hedgehog meron could ever exist by pairing with another type of meron. Using element-resolved magnetic imaging measurement on epitaxial trilayer disks, we show that a spin meron with a full range of helicity, including the hedgehog meron, can be stabilized by pairing with another vortex meron with a fine tuning of the magnetic coupling between the two merons. Furthermore, the meron divergence is fully controlled by the polarity of the vortex meron, independent of the vortex helicity.

PACS: 72.25.Mk, 72.15.-v, 78.47.db

1. Introduction

Meron was described originally in the context of quark confinement as one-half of a topological unit and can exist only in pairs [1]. In condensed matter physics, a spin meron corresponds to one-half of a spin skyrmion which carries one unit topological charge [2,3]. While spin skyrmions have been proposed [4,5] and realized recently in experiments [6,7] with many fascinating topological properties [8,9], it remains a mystery on why single hedgehog spin meron has never been discovered although a magnetic vortex [10] has been argued to be a vortex-type spin meron [11]. Noticing that vortex-type (spins curling around a center) and hedgehog-type (spins diverge/converge from a center) skyrmions have different helicities (γ, defined as the whirling angle of a spin texture from a divergent structure) [8], the role of the helicity in the formation of the spin merons has been speculated on. Although a helicity change doesn't change the topology of a spin texture, it was found recently that the helicity actually plays a critical important role in many skyrmion topological properties. For example, Nomura *et al.* showed that electric charge can be induced in hedgehog-type ($\gamma = 0, \pi$) spin textures on top of a topological insulator and subsequently affects the domain wall motions [12]. Yokoyama *et al.* proposed that the supercurrent in a superconductor/magnetic skyrmion/superconductor junction can be controlled by the helicity of the magnetic skyrmion [13]. Rowland *et al.* suggest that the skyrmion phase in a skyrmion crystal could be significantly expanded by changing the helicity from the vortex-type ($\gamma = \pm\pi/2$) in the Dresselhaus limit to the hedgehog-type ($\gamma = 0, \pi$) in the Rashba limit [14]. The above results on skyrmion research suggest that the helicity may also play a critical role in the formation of spin merons. Since the helicity is directly related to the magnetic charge in a magnetic system especially the magnetic surface charge at the boundary of a finite magnetic system, it has been speculated that hedgehog merons can only exist in pairs via a spin flux closure between the two merons. First evidence on the existence of hedgehog meron pairs comes from a study on a magnetic trilayer disk where two ferromagnetic (FM) disks are antiferromagnetically (AFM) coupled through a spacer layer [15]. Direct proof of the hedgehog-like meron pair structure, however, was provided only by using element-resolved magnetic imaging [16]. It was shown that the spin flux closure leads to an antisymmetric relation in the divergence and circulation of the two merons. On the other hand, recent result on magnetic bilayers showed that spin merons in one magnetic film can only be partially replicated in the second magnetic layer [17]. The above results raise a critical issue: does a hedgehog meron have to be paired with another hedgehog meron of opposite helicity (i.e., opposite divergence and circulation)? Or alternatively, can a hedgehog meron be stabilized by pairing it with another type of meron (e.g. vortex meron)? In this paper, we report our result on the study of epitaxially grown trilayer disks in which two FM disks are coupled through a spacer layer. By synthesizing asymmetric trilayer disks in which one FM disk is forced to form a vortex meron, we are able to fully explore the meron state of the second FM disk as a function of the magnetic interlayer coupling between the two FM disks. We demonstrate that the second meron can be stabilized from the vortex-type to the hedgehog-type merons in the full range of helicity. In particular, a hedgehog meron could be stabilized by pairing with a vortex meron without the need of spin flux closure. In addition, we show that the divergence of the hedgehog meron is solely determined by

the polarity of the vortex meron, independent of the vortex circulation.

2. Experiment

The Ni/Fe/Co trilayers were grown epitaxially at room temperature in an ultrahigh vacuum (UHV) chamber with a base pressure of 1×10^{-10} Torr. A Cu(001) substrate was treated in the ultrahigh vacuum chamber by cycles of Ar ion sputtering at 2 keV and annealing at 600℃. The Ni and Co thicknesses were fixed at 5ML and 150ML, respectively. The Fe spacer layer was grown into a wedge shape with its thickness varying continuously from 5ML to 6ML over ~0.5mm lateral distance. Circular disks of 0.75 μm radius were deposited in the central area of the Cu substrate using a contact shadow mask, and continuous films were deposited outside the shadow mask region. Because of the small slope of the wedge (2ML/mm), the Fe spacer layer thickness is virtually the same in each disk but varies from disk to disk continuously from 5ML to 6ML. 11ML of Cu was deposited as a capping layer to protect the sample from oxidization. It is well known that Ni and Co on Cu(001) have face-centered-cubic (fcc) structure exhibiting a FM order independent of layer thickness [18,19]. Fe films on Cu(001), however, have an fcc structure below 11ML with its magnetic phase being FM for $d_{Fe} < 4$ML and AFM for $4 < d_{Fe} < 11$ML [20]. Same results were also observed for Fe/Co/Cu(001) [21] and Ni/Fe/Cu(001) [22]. Low Energy Electron Diffraction was used to characterize the sample, and confirms the formation of fcc Ni, Fe, and Co films on Cu(001) [FIG. 1(c)]. Element-resolved X-ray Magnetic Circular Dichroism (XMCD) measurement was performed on the Co, Fe, and Ni 2p level at the Advanced Light Source of Lawrence Berkeley National Laboratory. Magnetic measurements of the Ni/Fe/Co sandwich were from the same sample, with the hysteresis loops taken on the continuous film at BL4.0.2 and magnetic images of the disks taken using Photoemission Electron Microscopy (PEEM) at BL11.0.1.

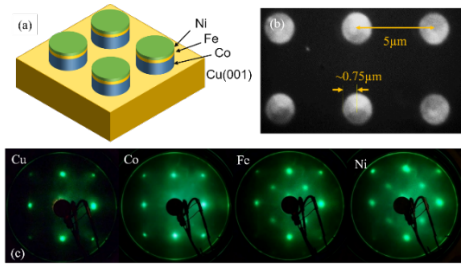

FIG. 1. (Color online) (a) Schematic drawing of the Ni/Fe/Co/Cu(001) trilayer disks in which the ferromagnetic Ni and Co are magnetically coupled across the antiferromagnetic fcc Fe spacer layer. (b) PEEM image of the Ni/Fe/Co/Cu(001) trilayer disks. (c) LEED patterns from each stage of the Ni(5ML)/Fe(wedge)/Co(150ML)/Cu(001) film growth confirm the epitaxial growth of fcc Ni, Fe, and Co single crystalline films.

3. Results and Discussion

3.1 Magnetic Interlayer Coupling

It is well known that magnetic interlayer coupling between two FM films across a non-FM spacer layer oscillates between FM and AFM couplings with the spacer layer thickness [23]. Thus the interlayer coupling between the FM Ni and Co layers in our Ni/Fe/Co/Cu(001) trilayers is expected to oscillate with increasing the AFM fcc Fe spacer layer thickness [24]. We studied the interlayer coupling by performing element-resolved hysteresis loop measurements using the total electron yield X-ray absorption at the L_3 edges of Co and Ni layers at different Fe thickness (FIG. 2). At $d_{Fe} = 6\ ML$, the hysteresis loops of both Co and Ni have the same shape and identical coercivity, showing a FM coupling between the Ni and Co magnetizations. At $d_{Fe} = 5\ ML$, the Co magnetization shows the typical hysteresis loop with its magnetization aligned to the magnetic field direction above the coercivity. The Ni hysteresis loop, however, 'saturates' in the opposite direction of the magnetic field (e.g., the Ni magnetization is aligned antiparallel to the Co magnetization), showing an AFM coupling between the Ni and Co magnetizations. Moreover, the opposite alignment between the Ni magnetization and magnetic field shows that the Ni-Co AFM coupling is stronger than the Ni Zeeman energy for magnetic field at least up to 0.1 T. The Ni magnetization actually increases linearly above the coercivity with increasing magnetic field, and should eventually align to the magnetic field direction at strong enough field when the Zeeman energy overcomes the Ni-Co AFM coupling. From the linear slope of the Ni magnetization above the coercivity in FIG. 2a, we could extrapolate that it takes about H~3.5 T to overcome the Ni/Co AFM coupling to align the Ni magnetization to the magnetic field direction.

We estimate the strength of the magnetic interlayer coupling constants as follows. The interlayer coupling energy per unit area can be written phenomenologically as [25,26]:

$$E_{IC} = -J_L \frac{\vec{M}_{Ni}\cdot\vec{M}_{Co}}{M_{Ni}M_{Co}} - J_Q\left(\frac{\vec{M}_{Ni}\cdot\vec{M}_{Co}}{M_{Ni}M_{Co}}\right)^2$$
$$= -J_L\, cos(\theta_{Co}-\theta_{Ni}) - J_Q\, cos^2(\theta_{Co}-\theta_{Ni})$$

Here θ_{Co} and θ_{Ni} denote the Co and Ni magnetization orientations, respectively. The bilinear coupling $J_L > 0$ (or $J_L < 0$) favors a ferromagnetic (or antiferromagnetic) alignment and the so-called biquadratic coupling of $J_Q < 0$ favors an orthogonal ($\theta_{Co} - \theta_{Ni} = \pm\pi/2$) alignment of the Ni and Co magnetizations, respectively. Then the total energy per unit area of the trilayer within an applied magnetic field H is:

$$E = -M_{Ni}d_{Ni}H\cos(\phi_H - \theta_{Ni}) - M_{Co}d_{Co}H\cos(\phi_H - \theta_{Co}) - J_L\cos(\theta_{Co} - \theta_{Ni}) - J_Q\cos^2(\theta_{Co} - \theta_{Ni})$$

We have ignored the anisotropy terms here to best single out the effect of the magnetic interlayer coupling. This is justified when the interlayer coupling dominates the anisotropy energy. Since the thickness of Co is much greater than Ni, the Co magnetization is approximately parallel to the applied field direction. Then by setting $\theta_{Co} = \phi_H$, we have:

$$E = -M_{Ni}d_{Ni}H\cos(\phi_H - \theta_{Ni}) - M_{Co}d_{Co}H - J_L\cos(\phi_H - \theta_{Ni}) - J_Q\cos^2(\phi_H - \theta_{Ni})$$

Minimizing the total energy by $\frac{dE}{d\theta_{Ni}} = 0$, we derive the Ni magnetization angle:

$$-M_{Ni}d_{Ni}H - J_L - 2J_Q\cos(\phi_H - \theta_{Ni}) = 0$$

Note that $\phi_H = 0$ for $H > 0$ and $\phi_H = \pi$ for $H < 0$ during the hysteresis loop measurement, then we have:

$$\cos\theta_{Ni} = \begin{cases} \frac{-J_L - M_{Ni}d_{Ni}H}{2J_Q} & for\ H > 0 \\ \frac{+J_L - M_{Ni}d_{Ni}H}{2J_Q} & for\ H < 0 \end{cases} \quad (1)$$

provided that $|\cos\theta_{Ni}| \leq 1$ (e.g., bounded by the saturation field).

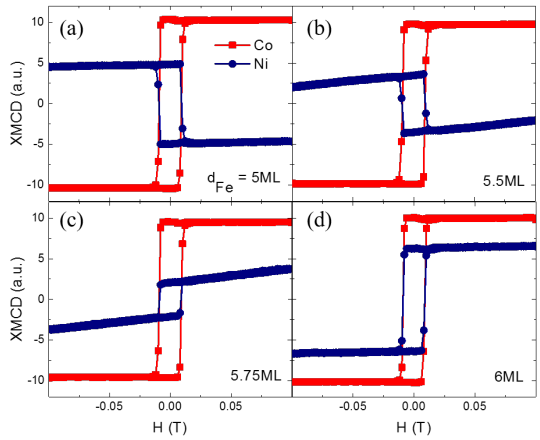

FIG. 2. (Color online) Element-resolved hysteresis loops of Ni(5ML)/Fe/Co(150ML)/Cu(001). (a) $d_{Fe} = 5\ ML$, (b) $d_{Fe} = 5.5\ ML$, (c) $d_{Fe} = 5.75\ ML$ and (d) $d_{Fe} = 6\ ML$. The Ni magnetization saturates in the opposite direction of Co at $d_{Fe} = 5\ ML$, indicating a strong antiferromagnetic interlayer coupling between the Ni and Co magnetizations. The Ni and Co have identical shape of hysteresis loops at $d_{Fe} = 6\ ML$, indicating a ferromagnetic interlayer coupling between the Ni and Co magnetizations. The linear slopes in Ni hysteresis loops above the coercivity are described by eqn. (1).

This equation gives us the component of Ni magnetization along the applied field direction, which is the linear portion of the Ni hysteresis loops in FIG. 2. With known values of $M_{Ni} = 4.9\times10^5\frac{A}{m}$ and $d_{Ni} = 1\ nm$, we fit the linear portion of the Ni hysteresis loops at four different Fe thicknesses and obtain the following bilinear and biquadratic coupling strengths with estimated error of $\pm0.01\ mJ/m^2$ (Table 1):

Table 1 | Bilinear and biquadratic coupling strengths.

$d_{Fe}(ML)$	$J_L(mJ/m^2)$	$J_Q(mJ/m^2)$
5	< -0.68	-0.34
5.5	-0.13	-0.09
5.75	$+0.06$	-0.07
6	$> +1.02$	-0.51

At the remanent state, minimizing the interlayer coupling energy leads to different coupling angles of $\Delta\theta = \theta_{Ni} - \theta_{Co}$ at different relative strengths of J_L and J_Q, summarized as follows for $J_Q < 0$:

$$J_L > 2|J_Q|, \Delta\theta = 0$$
$$J_L < -2|J_Q|, \Delta\theta = \pi$$
$$-2|J_Q| < J_L < 2|J_Q|, 0 < \Delta\theta < \pi \quad (2)$$

From the J_L and J_Q values obtained from the hysteresis loops, we expect a full range of $0 < \Delta\theta < \pi$ in our system [27]. Adding a 4-fold magnetic anisotropy will modify the formula a little but won't alter the result that, as the bilinear coupling changes from ferromagnetic to antiferromagnetic coupling, the coupling angle $\Delta\theta$ changes continuously from 0 to π at the presence of a biquadratic coupling, permitting a full exploration of the Ni-Co meron pair formation in Ni/Fe/Co disks as we will demonstrate.

3.2 Domain images of Ni/Fe/Co trilayer disks

In our sample of Ni(5ML)/Fe/Cu(150ML) disks, the thick Co disk in the trilayer should behave similar to a single Co disk to form a vortex meron. PEEM imaging measurement shows that the Co disk indeed forms the magnetic vortex meron ($\gamma_{Co} = \pm\pi/2$) in the trilayer disks with the Co spins curling around the disk center along the four equivalent [110] magnetization easy axes (FIG. 3a–e). No hedgehog merons were found in the Co disk for all Fe thicknesses studied. In contrast, the Ni disk exhibits a variety of meron states at different Fe thicknesses. At $d_{Fe} = 5\ ML$, the Ni disk forms a vortex meron (FIG. 3a) with it helicity opposite to that of Co disk ($\gamma_{Ni} = -\gamma_{Co}$). This is because

the strong AFM coupling between the Ni and Co magnetizations at $d_{Fe} = 5\,ML$ (FIG. 2) favors an antiparallel alignment of the Ni and Co magnetization directions. Similarly, the Ni disk also forms a vortex meron (FIG. 3j) at $d_{Fe} = 6\,ML$ with its helicity the same as that of Co ($\gamma_{Ni} = +\gamma_{Co}$) because of the strong FM interlayer coupling between Ni and Co magnetizations. The most interesting observation is that the Ni meron state undergoes a drastic change (FIG. 3g–i) with increasing Fe thicknesses. From the Ni domain XMCD contrast, we find that assuming the same Co-Ni coupling angle within a single disk the Ni spin direction (the colored arrows in Figure 3) changes continuously from $\pm\pi$ (AFM coupling) to 0 (FM coupling) relative to the Co spin direction with increasing the Fe thicknesses from 5ML to 6ML. In particular, we found that Ni hedgehog meron ($\gamma_{Ni} = 0, \pm\pi$) could be stabilized with the Co vortex meron ($\gamma_{Co} = \pm\pi/2$) to form a hedgehog/vortex meron pair which has never been discovered before. The distortion in some of the Ni domains (e.g., the edge in Figure 3i) is perhaps due to the imperfection of the sample fabrication using the shadow mask which disturbs the domain more easily in thin film (Ni) than thick film (Co). Our result shows that the Ni helicity can be tuned in the full range of 0 to $\pm\pi$ by the magnetic interlayer coupling without the need of Dzyaloshinskii-Moriya interaction [28,29]. Furthermore, we found no correlation between the divergence ($d = +1$ for divergence, and $d = -1$ for convergence) of the Ni hedgehog meron and the circulation ($c = 1$ for counter-clockwise, and $c = -1$ clockwise) of the Co vortex meron. It should be mentioned that XMCD measures magnetization along the X-ray direction so that only the horizontal components of the magnetization is captured in FIG. 3. In another word, we can determine cosϕ from the XMCD values of the Ni domain quadrants, where ϕ is the angle between the Ni magnetization and the horizontal direction, but not the sign of ϕ. Therefore, although the blue and red arrows in the Ni domain can be determined by experiment, the divergent/convergent component of the yellow and green arrows cannot be determined due to instrumental limitation in the current experiment (e.g. *in situ* rotation of the sample by 90 degrees). However, our simulation results and symmetry arguments (see section 3.3) show that anti-meron state (winding number $w = -1$) is highly unfavored. Then the helicity γ was deduced from the XMCD values which were determined by the averaged value in each of the quadrants of the Ni domains.

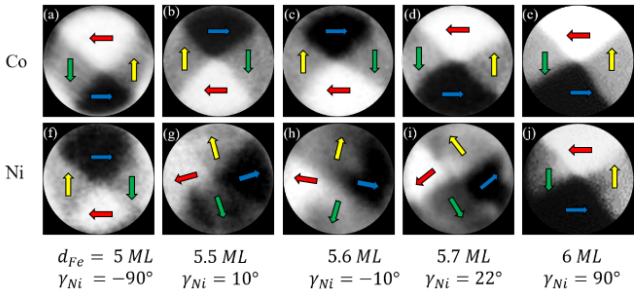

FIG. 3. (Color online) Element-resolved magnetic images of Ni and Co in Ni/Fe/Co/Cu(001) single crystalline disks. (a) - (e) Co always forms a vortex meron with the magnetization curling along four equivalent [110] easy magnetization axes. (f) – (j) Ni domain shapes follow that of Co but the Ni helicities change continuously from $\gamma_{Ni} = -\pi/2$ to $\gamma_{Ni} = +\pi/2$ with increasing the fcc AFM Fe thickness, showing a full range of the Ni helicity control by the magnetic interlayer coupling.

The above result can be understood qualitatively by recalling that different helicities lead to different magnetic charges ($\rho_B = -\nabla \cdot \vec{M},\ \sigma_B = -\vec{M} \cdot \hat{n}$) in a FM disk, where $\vec{M}$ is the magnetization, $\hat{n}$ is the unit vector in the normal direction of the disk's edge surface, and ρ_B and σ_B are the volume and surface magnetic charge densities, respectively. It is known that a curling structure of spins (vortex meron) could minimize the magnetostatic energy by minimizing the magnetic surface charges at the disk boundary, thus permitting the formation of single vortex meron in a FM disk. In contrast, a divergent structure of spins (hedgehog meron) would increase the magnetostatic energy due to the exposure of the magnetic charges at the disk boundary, thus forbidding the formation of single hedgehog meron in a FM disk. However, it is possible to lower the magnetostatic energy by the magnetic charge-charge attraction between two hedgehog merons carrying opposite magnetic charges, thus favoring the formation of hedgehog meron pairs in a trilayer disk. In literature, such spin textures with radially diverging/converging spins have been referred to as a 'meronlike'-state [15] or effective merons [16], and indeed obey the spin flux closure relation in the divergence and circulation of the two merons ($d_1 = -d_2;\ c_1 = -c_2$) in trilayer disks of similar FM disk thicknesses. On the other hand, this mechanism also limits the accessible helicity of meron pairs because both merons have to change simultaneously with respect the change of the interlayer coupling. In our system, the Co disk is much thicker than the Ni disk so that the Co vortex meron is virtually unaffected by the Ni meron state. In contrast, the Ni disk has a much less magnetic surface charge at the disk edge because of its ultrathin thickness so that its magnetization direction is almost completely determined by its magnetic coupling to the Co layer. That is why a single hedgehog meron in the Ni disk can be stabilized with the Co vortex

meron in our system under a biquadratic coupling between the Ni and Co layers. In fact, the interlayer coupling angle between Ni and Co magnetizations changes continuously from 0 to π as the Fe thickness changes between 5 and 6 ML. Thus the Ni meron helicity could change continuously in the full range without the need of an opposite circulation to that of Co. Using micromagnetic simulations, we confirm that these configurations (divergent/convergent, left/right circulation merons) are indeed energetically stable states in the Ni disk (see section 3.4). Hence we showed that it is not necessary for both merons to have non-zero divergence as long as the interlayer exchange coupling dominates the total energy of the trilayer in an asymmetric sample structure.

3.3 Topological Imprinting

Since the interlayer coupling energy depends only on the angle between the two FM layer magnetizations, there are two degenerate configurations at any given interlayer coupling which correspond to a clockwise and counter-clockwise rotation of the Ni magnetization with respect to the Co magnetization ($\gamma_{Ni} = \gamma_{Co} \pm \Delta\gamma$ for a given $\Delta\gamma$) respectively. Therefore except the special cases of $\Delta\gamma = 0$ or π, there should be always two Ni configurations of $\pm\Delta\gamma$ at any local position of the trilayer disk, leading to $2^4 = 16$ possible configurations for the imprinted Ni domains with each of the 4 domain regions having two possibilities of $\gamma_{Ni} = \gamma_{Co} \pm \Delta\gamma$. The 16 possible configurations are enumerated in the sketch of

FIG. *4* for an arbitrary coupling angle. Of these 16 possible configurations that are congruent with the Co vortex only 2 of them have the same winding number (w) as Co. Micromagnetic simulations show that configurations with different winding number from the Co will lead to Ni spins at the domain walls having a different coupling angle thus resulting in a higher coupling energy. The winding number of the imprinted domain pattern must follow that of the Co layer.

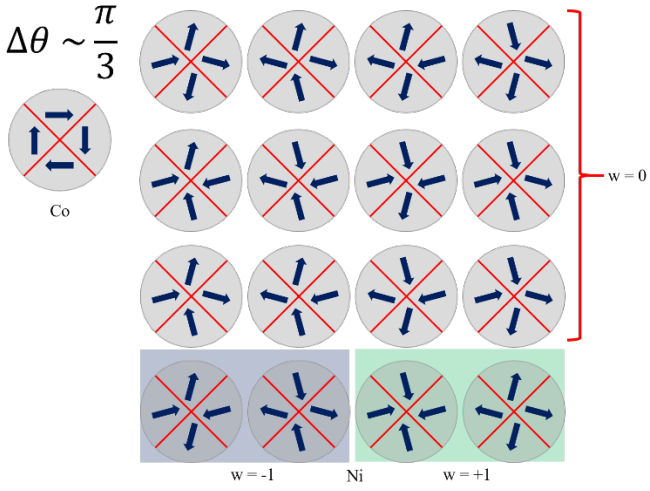

FIG. 4. (Color online) At any given coupling angle ($\Delta\theta = \pi/3$ in this figure) between Ni and Co magnetizations, there are $2^4 = 16$ possible Ni meron configurations resulting from the same Co vortex state, of which only 2 have the same winding number ($w = +1$) as Co.

Using micromagnetic simulation, we found that even if we initialize the thin ferromagnetic Ni layer into an anti-meron state with a winding number of $w = -1$, it will quickly relax to a configuration with the winding number of $w = +1$, the same as that of the Co layer vortex, i.e. $\Delta\gamma$ should not switch its sign within the Ni disk from location to location. For example, at $\pi/2$-degree coupling angle between the Ni and Co magnetizations, the spins in the Ni disk (FIG. 5) should be either all divergent ($\gamma_{Ni} = 0$) or all convergent ($\gamma_{Ni} = \pm\pi$) but not a mixture of divergent/convergent (e.g., not an anti-meron where the spins are divergent in two directions and convergent in the orthogonal two directions). This result shows that as the Co disk imprints the spin texture into the Ni disk through the magnetic interlayer coupling, the topological winding number [8] of the Co vortex meron is preserved and carried over into the Ni meron, similar to bilayer skyrmion imprinting [30,31].

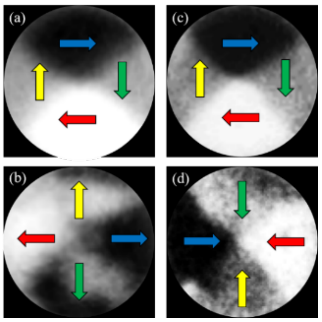

FIG. 5. (Color online) Hedgehog/Vortex meron pairs in Ni/Fe(5.55ML)/Co/Cu(001) disks. (a) and (c) Co disk exhibits vortex meron state, and (b) and (d) Ni disk exhibits hedgehog meron state with either divergent structure for p=+1 core polarity or convergent structure for p=-1 core polarity.

It should be mentioned that the observed Ni hedgehog meron domains look more complicated than described in

FIG. *4*, especially near the edges of the disks. These imperfections vary from disk to disk (

FIG. *6*). We believe there are two possible reasons. First, from measurement point of view, the PEEM measurement is based on electron emission so that the edges of the sample (such as from our disk) could affect or distort significantly the emission intensity. This effect does not exist for flat continuous films but becomes significant for ultrathin microstructures. For thick Co such effect is less

significant because of the strong XMCD signal. For ultrathin Ni (5ML) disk, however, such effect often influences the uniformity of the domain contrast and even distort the PEEM domain images from small patterned structures. Second, monolayer thick magnetic domains are disturbed easily by any impurities such as dusts on the surface. That's why there is very few, if any, monolayer thick domain images from microstructures made by lithography because the left over chemical materials often disturb the monolayer thick domain structures. This effect could be more pronounced for energetically degenerate states in monolayer thick microstructures, such as $\pm\Delta\gamma$ states in our Ni merons. In addition, by comparing Fig. 3 and Fig. 6, we find that both divergent and convergent Ni merons could be formed for the same circulation of the Co vortex, i.e., there is no correlation between the Co vortex meron circulation and the convergence/divergence of the corresponding Ni merons.

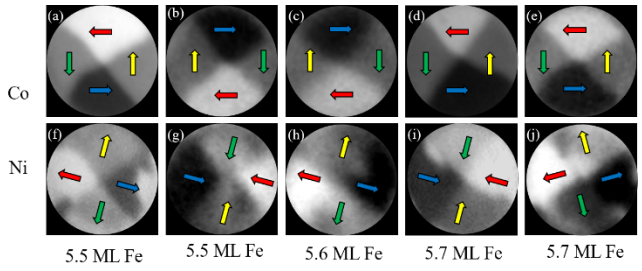

FIG. 6. (Color online) Element-resolved magnetic images of Ni and Co in Ni/Fe/Co/Cu(001) single crystalline disks. (a) - (e) Co disks always form vortex merons. (f) – (j) Ni disks form hedgehog merons that vary from disk to disk. There is no correlation between the circulation of Co vortex merons with the convergence/divergence of the corresponding Ni hedgehog merons.

3.4 Micromagnetic Simulations

Then the interesting question is: what determines the Ni meron divergence? In a trilayer with comparable FM disk thicknesses, the divergence of one meron is always accompanied with the convergence of another meron. Magnetic simulation result shows that the divergence of the meron is determined by the polarity of the meron pairs. The above results has been attributed to the spin flux closure mechanism [16]. In our system, the Co disk is always a vortex meron and we find no correlation between the Ni divergence and the Co vortex circulation direction. Therefore the in-plane spins of the Co vortex do not play any role in the Ni meron divergence. Noting that a single meron should not have the divergence/polarity correlation because of the up/down symmetry, we believe that the divergence/polarity correlation in the trilayer disk originates from the interaction between the Ni in-plane spins and the Co vortex core. We recall that a magnetic vortex meron consists of in-plane spins curling around an out-of-plane spin core. A vortex meron generates a stray magnetic field similar to a field from a magnetic dipole moment that is located at the vortex core and points in the same direction as the vortex core polarity. Therefore the Ni meron in the Ni/Fe/Co disk is actually placed above a dipole moment from the Co vortex core. This Co dipole moment, whose magnitude scales with the core volume (core area times the Co thickness), below the Ni disk should align not only the Ni out-of-plane core polarity to the same direction of the Co polarity but also the in-plane radial component of the Ni spins to the radial component of the Co dipole field at the Ni disk, leading to a positive or negative divergence of the Ni meron ($d_{Ni} = +1\ or\ -1$) for Co out-of-plane core polarity pointing towards the Ni disk ($p_{Co} = +1$) or away from the Ni disk ($p_{Co} = -1$). Note that Co dipole field has no effect on the tangential component of the Ni spins, neither does it depend on its own tangential spins. That is why we observed no correlation between the circulations, neither any correlation between the Ni divergence and the Co circulation, in our Ni/Co meron pair. To test the divergence/polarity correlation, we performed a series of micromagnetic simulations using the Object Oriented MicroMagnetic Framework code based on the Landau–Lifshitz–Gilbert equation. The following magnetic materials parameters are used in all simulations presented in this work: Saturation magnetization $M_{Co} = 1.4\times10^{6} Am^{-1}$, exchange stiffness $A_{Co} = 3\times10^{-11} Jm^{-1}$ for the Co layer, and $M_{Ni} = 4.9\times10^{5} Am^{-1}$, $A_{Ni} = 1.2\times10^{-11} Jm^{-1}$ for the Ni layer. The diameter of the coupled disks are set to be 1 μm.

Hedgehog meron formation in Ni/Fe/Co trilayer disks

We confirmed that Ni hedgehog merons could be stabilized in a coupled trilayer disks.

FIG. 7 shows stable Co and Ni domains coupled by a bilinear coupling of $4\times10^{-4} J/m^{2}$ and a biquadratic coupling of $-4\times10^{-4} J/m^{2}$. A fourfold magnetic anisotropy of $K_{Co} = 8\times10^{4} Jm^{-3}$ were used in the simulation to resemble the experimental conditions more closely. The simulation result shows that the Co disk always forms vortex state. The Ni disk always ends up as either convergent or divergent hedgehog meron state, but never as an anti-meron.

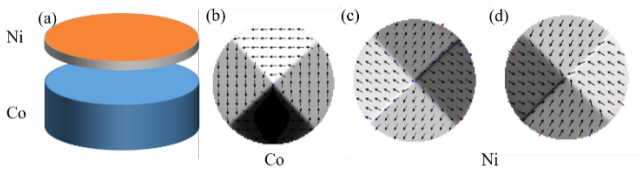

FIG. 7. (Color online) (a) Sketch of the sample geometry used in the micromagnetic simulation. (b) - (d) shows typical micromagnetic simulation results using Object Oriented MicroMagnetic Framework (OOMMF) package

[32]. Both divergent and convergent meron states can be stabilized in the Ni disk while the much thicker Co disk retains a vortex meron state The grayscale color is used here to emulate the measurement results from PEEM, which is sensitive only to magnetization along x-ray direction.

Stray magnetic field from a Co vortex meron

To show that the stray field from a vortex meron is similar to a field from a dipole moment, we performed a micromagnetic simulation to calculate the stray magnetic field from a 50nm thick Co disk of 500nm radius. We chose a polarity of p=+1 for the simulation and a cell size of $2\times2\times2\ nm$ for the stray field calculation. The stray field resulting from this Co disk at a position 1.5 nm above the disk top surface (where the Ni disk would have been in the actual experiment) is shown in

FIG. *8*. First, we find that both right- and left-circulated vortex merons produce the same stray magnetic field (

FIG. *8*a and b), confirming that the stray field is mostly generated by the vortex core and is independent of the circulation. Second, the in-plane stray field is always divergent for p=+1 even when the out-of-plane component of the stray field could change from +z direction (red colored region) to –z direction (blue colored region).

FIG. *8*c shows the stray field from a single magnetic dipole moment (pointing to the +z direction) placed ~17nm below the calculated surface. The result represents the actual stray field from the Co vortex meron well, confirming that the stray field of a vortex meron is equivalent to the stray field from a dipole moment. The position of 17nm distance below the surface is above the center of the Co disk which is 26.5nm below the calculated surface. This is because a magnetic moment closer to the surface contributes to the field more than a moment further away from the surface.

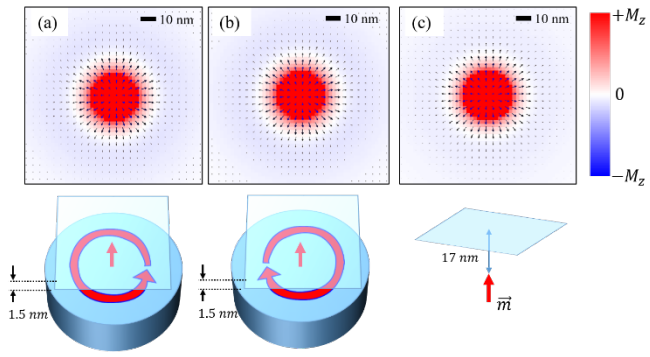

FIG. 8. (Color online) Micromagnetic simulation of of the stray field from the Co vortex meron with out-of-plane polarity at a position 1.5 nm above the Co disk top surface. The arrows indicate the in-plane component of the stray magnetic field. The red and blue colors indicate the out-of-plane stray magnetic field component. (a) From right-handed circulation disk. (b) From left-handed circulation disk. (c) From a single magnetic moment positioned ~17nm below the calculated surface.

Energy difference between divergent and convergent merons

To calculate the energy difference between the divergent and convergent Ni meron with a fixed Co meron vortex core polarity, we performed micromagnetic simulations with various thicknesses of Ni. The cell size used for these set of simulations is $5\times5\times0.5\ nm$. The bilinear and biquadratic interlayer exchange coupling constants are set to $J_L = 0$ and $J_Q = -5\times10^{-4} Jm^{-2}$ so that the coupling angle between Co and Ni is set at $\Delta\gamma = \pi/2$ to manifest the divergence/polarity correlation (the result won't change at $\Delta\gamma \neq \pi/2$). For a fixed Co vortex core polarity, we found that the Ni meron always has its core polarity the same as the Co, i.e., a Ni meron cannot be stabilized with its core polarity opposite to the Co core polarity. Under the condition of the same Ni and Co core polarity, we found that both $+\Delta\gamma$ and $-\Delta\gamma$ Ni meron states can be stabilized as metastable states. However, the lower energy state always has a divergent (convergent) structure for up (down) polarity of the meron core. FIG. 9 shows the energy difference (ΔE) between these two states for different Ni thickness (d_{Ni}) at a fixed Co thickness of $d_{Co} = 50\ nm$. The ΔE value increases almost linearly with the Ni thickness. Note that the anisotropies of Co and Ni are ignored in this set of simulations since we're only interested in a qualitative picture of the energy difference between the $\pm\Delta\gamma$ two states.

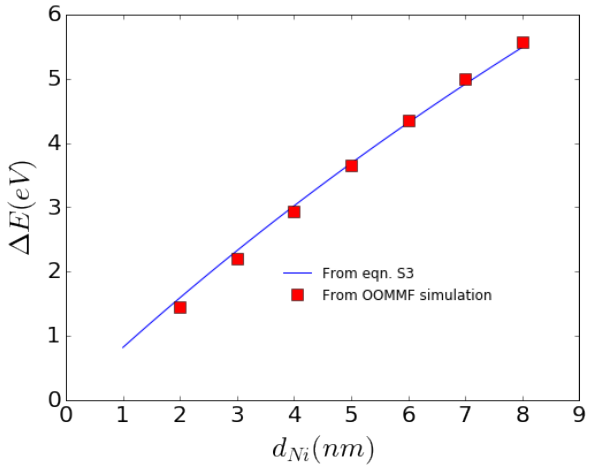

FIG. 9. (Color online) Energy difference between convergent and divergent meron states as a function of Ni thickness. The red squares are from OOMMF simulations. The blue line is from eqn. (3) of the simplified model.

The linear dependence in FIG. 9 is consistent with the physical picture described in the main text that the Ni spin divergence (convergence) is a result of the dipole interaction between the Ni spins and the Co vortex core dipole moment. To further confirm this physical picture, we consider the following over simplified model where the effective magnetic dipole moment of the Co vortex core is described approximately by $\vec{m}_{Co} = M_{Co}\pi\delta^2 d_{Co}\,\hat{z}$, δ is the radius of the Co vortex core, and d_{Co} is the thickness of the Co disk. This Co effective dipole moment is located at a distance s below the Ni core. Noticing that the difference between the convergent and divergent Ni meron states is simply reversing the in-plane spin direction outside the core, then the energy difference between the convergent and divergent Ni meron states is approximately

$$\begin{aligned}\Delta E &\approx \int_{\delta}^{R} 2\pi\rho d\rho \frac{\mu_0}{4\pi|\vec{r}|^3}\left(3(\vec{m}_{Co}\cdot\hat{r})(\Delta\vec{m}_{Ni}\cdot\hat{r}) - \vec{m}_{Co}\cdot\Delta\vec{m}_{Ni}\right)\\ &= \frac{3\mu_0}{2\pi} M_{Co}\pi\delta^2 d_{Co} M_{Ni} d_{Ni}\int_{\delta}^{R}\frac{s2\pi\rho^2}{(\rho^2+s^2)^{\frac{5}{2}}}d\rho\\ &= 3\pi\mu_0 M_{Co} M_{Ni}\delta^2 d_{Co} d_{Ni}\frac{1}{s}\left(\frac{\delta^3}{(\delta^2+s^2)^{\frac{3}{2}}} - \frac{R^3}{(R^2+s^2)^{\frac{3}{2}}}\right) \qquad (3)\end{aligned}$$

This equation gives rise approximately to a linear dependence on d_{Ni}. Using $R = 500\,nm$ for the disk radius, $d_{Co} = 50\,nm$, and $s = 17nm + d_{Ni}/2$ as the approximate distance of the effective Co moment below the Ni disk, the calculated ΔE as a function of d_{Ni} (blue curve in FIG. 9) could reproduce the simulation result very well at the value of $\delta \approx 5.2\,nm$ which agrees well with the Co vortex core size. For this energy difference to be able to separate the convergent and divergent meron states in experiment, the energy difference (ΔE_l) by flipping a block of spins from divergent to convergent over a characteristic length scale of l must be greater than the thermal excitation energy of $k_B T$. At 5ML Ni thickness, $\Delta E \approx 1\,eV$ so that the order of magnitude of ΔE_l can be roughly estimated to be $\Delta E_l \approx \Delta E \cdot l^2/R^2$. In experiment, we found that the divergence/polarity correlation is more significant at low temperature (T~100K) than room temperature (T=300K) where the thermal excitations start to fluctuate the meron state. Therefore, taking T=300K, we estimate that the length scale of the Ni spin fluctuation needs to be at least $l \sim R\sqrt{k_B T/\Delta E} \sim 80\,nm$ to manifest the divergence/polarity correlation. Of course the real physical process of thermal flipping of the Ni spins should be more complicated than the above over simplified estimation. Future theoretical studies are obviously needed to address such thermal flipping process of the meron states. To support this simulation result, we applied a ±2T out-of-plane magnetic field to align the vortex core before collecting the domain images [30]. Since the Curie temperature of ~5ML Ni film is very close to room temperature, we demagnetized the sample at ~100K to reduce thermal fluctuations in order to reach the ground state of the merons. The result shows that most of Ni merons are divergent for the +2T pre magnetic field, and convergent for the -2T pre magnetic field.

4. Summary

In summary, we synthesized single crystalline Ni/Fe/Co/Cu(001) trilayer disks and investigated the formation of meron pairs in the Co and Ni disks. By employing asymmetric thickness to force the Co into a vortex meron state, we successfully achieved a full-range control of the helicity of the Ni meron by tuning the Ni-Co magnetic interlayer coupling across the fcc Fe spacer layer. In particular, we find that a single hedgehog meron could exist by pairing with a vortex meron. In addition, we find that the divergence/convergence of the Ni hedgehog meron is determined by the Co vortex core polarity, independent of its circulation.

Acknowledgments

Financial support through National Science Foundation DMR-1504568 and NRF through Global Research Laboratory project of Korea is gratefully acknowledged. The operations of the Advanced Light Source at Lawrence Berkeley National Laboratory are supported by the Director, Office of Science, Office of Basic Energy Sciences, and U.S. Department of Energy under contract No. DE-AC02-05CH11231.

References:

Correspondence and requests for materials should be addressed to J. Li at jiali83@pku.edu.cn.

[1] C. G. Callan, Jr., R. Dashen, and D. J. Gross, Phys. Rev. D 17, 2717 (1978).
[2] M. Ezawa, Phys. Rev. B 83, 100408 (2011).
[3] M. Pereiro, D. Yudin, J. Chico, C. Etz, O. Eriksson, and A. Bergman, Nat. Commun. **5,** 4815 (2014).
[4] U. K. Röβler, A. N. Bogdanov, and C. Pfleiderer, Nature 442, 797–801 (2006).
[5] L. Sun, R. X. Cao, B. F. Miao, Z. Feng, B. You, D. Wu, W. Zhang, A. Hu, and H. F. Ding, Phys. Rev. Lett. 110, 167201 (2013).
[6] S. Mühlbauer, B. Binz, F. Jonietz, C. Pfleiderer, A. Rosch, A. Neubauer, R. Georgii, and P. Böni Science 323, 915–919 (2009).
[7] W. Jiang, P. Upadhyaya, W. Zhang, G. Yu, M. B. Jungfleisch, F. Y. Fradin, J. E. Pearson, Y. Tserkovnyak, K. L. Wang, O. Heinonen, S. G. E. te Velthuis, and A. Hoffmann, Science 349, 283 (2015).
[8] H. B. Braun, Adv. Phys. 61, 1–116 (2012).
[9] N. Nagaosa and Y. Tokura, Nat. Nanotechnol. 8, 899–911 (2013).
[10] T. Shinjo, T. Okuno, R. Hassdorf, K. Shigeto, and T. Ono, Science 289, 930–932 (2000).

[11] O. Tretiakov and O. Tchernyshyov, Phys. Rev. B 75, 012408 (2007).
[12] K. Nomura and N. Nagaosa, Phys. Rev. B 82, 161401 (2010).
[13] T. Yokoyama and J. Linder, Phys. Rev. B 92, 060503 (2015).
[14] J. Rowland, S. Banerjee, and M. Randeria, Phys. Rev. B 93, 020404(R) (2016)
[15] C. Phatak, A. K. Petford-Long, and O. Heinonen, Phys. Rev. Lett. 108, 067205 (2012).
[16] S. Wintz, C. Bunce, A. Neudert, M. Körner, T. Strache, M. Buhl, A. Erbe, S. Gemming, J. Raabe, C. Quitmann, and J. Fassbender, Phys. Rev. Lett. 110, 177201 (2013).
[17] C. Blanco-Roldán, C. Quirós, A. Sorrentino, A. Hierro-Rodríguez, L. M. Álvarez-Prado, R. Valcárcel, M. Duch, N. Torras, J. Esteve, J. I. Martin, M. Vélez, J. M. Alameda, E. Pereiro, and S. Ferrer, Nat. Commun. **6**, 8196 (2015).
[18] B. Schulz and K. Baberschke, Phys. Rev. B **50**, 13467 (1994).
[19] C. M. Schneider, P. Bressler, P. Schuster, J. Kirschner, J. J. de Miguel, and R. Miranda, Phys. Rev. Lett. **64**, 1059 (1990).
[20] D. Li, M. Freitag, J. Pearson, Z. Q. Qiu, and S. D. Bader, Phys. Rev. Lett. **72**, 3112 (1994).
[21] E. J. Escorcia-Aparicio, R. K. Kawakami, and Z. Q. Qiu, Phys. Rev. B **54**, 4155 (1996).
[22] H. W. Zhao, C. Won, Y. Z. Wu, A. Scholl, A. Doran, and Z. Q. Qiu, Phys. Rev. B **70**, 024423 (2004).
[23] S. S. P. Parkin, N. More, and K. P. Roche, Phys. Rev. Lett. **64**, 2304 (1990).
[24] Y. Z. Wu, C. Won, A. Scholl, A. Doran, F. Toyoma, X. F. Jin, N. V. Smith, and Z. Q. Qiu, Phys. Rev. B **65**, 214417 (2002).
[25] J.C. Slonczewski, J. Magn. Magn. Mater. **150**, 13–24 (1995).
[26] D. Pierce, J. Unguris, R. Celotta, and M. Stiles, J. Magn. Magn. Mater. **200,** 290–321 (1999).
[27] J. C. Slonczewski, Phys. Rev. Lett. **67**, 3172 (1991).
[28] K. Shibata, X. Z. Yu, T. Hara, D. Morikawa, N. Kanazawa, K. Kimoto, S. Ishiwata, Y. Matsui, and Y. Tokura, Nat. Nanotechnol. **8,** 723–8 (2013).
[29] S. A. Díaz and R. E. Troncoso, arXiv:1511.04584
[30] J. Li, A. Tan, K. W. Moon, A. Doran, M. A. Marcus, A. T. Young, E. Arenholz, S. Ma, R. F. Yang, C. Hwang, and Z. Q. Qiu, Nat. Commun. **5,** 4704 (2014).
[31] D. A. Gilbert, B. B. Maranville, A. L. Balk, B. J. Kirby, P. Fischer, D. T. Pierce, J. Unguris, J. A. Borchers, and K. Liu, Nat. Commun. **6,** 8462 (2015).
[32] M. J. Donahue and D. G. Porter, OOMMF User's Guide Version 1.0 (National Institute of Standards and Technology, Gaithersburg, MD, 1999).